Experiments on an Unsteady, Three-dimensional Separation

R.W. Henk*, W.C. Reynolds† , and H.L. Reed‡
Stanford University, Stanford, California

Unsteady, three-dimensional flow separation occurs in a variety of technical situations, including turbomachinery and low-speed aircraft. An experimental program at Stanford in unsteady, three-dimensional, pressure-driven laminar separation has investigated the structure and time-scaling of these flows; of particular interest is the development, washout, and control of flow separation. Results reveal that a two-dimensional, laminar boundary layer passes through several stages on its way to a quasi-steady three-dimensional separation. The quasi-steady state of the separation embodies a complex, unsteady, vortical structure.

This talk will describe the experimental facility, the means of generating separation, and the stages of the development of an unsteady, three-dimensional separation.

Background

A working definition for three-dimensional separation has been adopted according to Legendre (1982) and Tobak and Peake (1982). Legendre (1982) succinctly states that a "line of separation ... has no local property. Its only characteristic is to pass through a saddle point." The definition stipulates that the reference frame is that of the surface and that the saddle point of the flow is on the surface. The three-dimensional separation generated in our experiment evolves into the type Owl face of the first kind according to the classification scheme by Perry and Hornung (1984). This separation has a clearly identifiable saddle point which was seen in visualizations of our flowfield. In this experiment the separation is seen to develop and decay in the reference frame of a fixed flat plate.

This experiment differs markedly from those by Didden and Ho (1985) and Koromilas and Telionis (1980). Didden and Ho report on an axisymmetric vortex traveling close to a wall. The MRS condition calls the contortions that the wall-jet boundary layer assume a *downstream-moving* separation (see Didden and Ho, 1985). In our experiment, *downstream-moving separation* refers to the decay of the separation as the sluggish fluid is sheared back into an unseparated velocity profile. The most important physics during this process is the diffusion of vorticity in the separated shear layer back to the surface.

Koromilas and Telionis (1980) documented the development of a two-dimensional separation. In their experiment, separation developed at the Howarth-flow section, where the test surface underwent deformation over time. A time-variation of the leading-edge vorticity and the test boundary layer accompanied this deformation. In our experiment, upstream conditions and the contours of the test surface remained constant. Our well-documented initial conditions and boundary conditions aid comparison with direct numerical simulations such as Pauley, *et al.* (1988).

---

* Graduate Student, Department of Mechanical Engineering, Stanford University.

† Professor, Department of Mechanical Engineering, Stanford University.

‡ Associate Professor, Department of Aeronautical and Mechanical Engineering, Arizona State University.

Experimental Facility and Experimental Conditions

The experimental facility is a closed-circuit water tunnel, figure 1, in which water flows from an overhead tank through the test section and then to a sump tank. Turbulence attenuation by honeycomb, screens, and acceleration through a nozzle provides a low turbulence freestream to the test section. A fresh boundary layer then develops under a zero pressure gradient until it reaches the unsteady portion of the test section. At this point, the boundary layer encounters either (1) a steady, zero or adverse pressure gradient, or (2) a computer-controlled, time-varying pressure gradient, as determined by the valves draining flow through the wall opposite the test surface. The water is continually pumped from the sump to the overhead tank to close the circuit.

The freestream flow is controlled by a bank of manual and computer-controlled valves located on the wall opposite the test surface. Typically the flow sees a zero pressure gradient. When instructed by the computer, some valves may be opened proportionately to create a local, adverse pressure gradient. The flowrate drained through each valve, and hence the imposed freestream flow, can be steady or unsteady. Any waveform may be imposed on the freestream flow. A square wave was chosen for these experiments.

For these experiments one upstream valve and one downstream valve are commanded to operate 180 degrees out of phase, producing a steady, zero pressure gradient flow in the upstream portion of the test section while the downstream flow sees an unsteady adverse pressure gradient. This ensures constant initial conditions for the test boundary layer; for example, leading-edge vorticity does not vary .

The test surface, a flat plate $2.7m$ long, forms the top wall of the test section. On the lower surface of the test surface, a fresh boundary layer is grown for investigation.

Laminar and turbulent boundary-layer experiments are performed in this tunnel. These laminar studies took place over the first meter of the test surface. The range of chord Reynolds numbers for the separation experiments extends from $1x10^5$ through $2x10^5$. Table 1 lists some of the flow parameters and geometry for this particular experiment.

Two laser doppler anemometer (LDA) systems measure velocities through the water tunnel. At the entrance to the test section, a single-component Helium-Neon LDA monitors the inlet flow. Downstream, the second LDA measures the velocity of the separated flow. This two-component Argon-Ion LDA is mounted on a traverse that permits movement of the measuring volume in all spatial directions. Motion normal to the test surface is automated for velocity surveys, which can continue for days without intervention.

Results: Stages in the development of a three-dimensional separation

The developing three-dimensional separation evolved through four distinct stages on its way to steady shedding. The four stages are the initial inviscid response, the breakaway of the shear layer, initiation of large-scale unsteadiness, and the quasi-steady state. Some zones of the separation structure experienced all of the stages as the separation develops under an impulsively imposed adverse pressure gradient.

Nomenclature for this section will use these special symbols: ⟨???⟩ refers to a phase-averaged quantity, where ??? is either a phase-mean velocity or double product term; LP:# refers to a measurement station along the centerline of the tunnel. Measurement

stations are shown in figure 2 with respect to tunnel geometry and the three-dimensional separation. Flow parameters and dimensions for tunnel geometry are listed in table 1.

The extent of each stage can be seen in a plot of the momentum-thickness histories at various locations along the centerline, figure 3. In the following subsections, the important features of each stage will be described more thoroughly.

Initial inviscid response. As is expected for an elliptic incompressible flow, flow through the entire tunnel responds instantaneously to the changes in the pressure gradient. Significant influence of the nonstationary, adverse pressure gradient is confined to downstream of $x \approx 0.55m$.

Breakaway of shear layer from the surface. The breakaway of the shear layer is part of the viscous response to the newly imposed adverse pressure gradient. It also contains aspects of an inviscid response as the near-wall flow is accelerated in the upstream direction. This can be modeled by taking the base case of a Blasius boundary layer and superimposing the potential flow correction.

It takes about $0.25s$ for the viscosity to catch up with the initial inviscid response. This stage at LP:1 lasts until $t \approx 4.5s$. The entire flow is remarkably quiescent throughout this stage of development. Figures 4a and 4b show phase-averaged $\langle U \rangle$-velocity profile histories at stations LP:1 and LP:2 respectively. The process that is taking place during this time is the displacement of the wall-bounded shear layer away from the surface as downstream and spanwise fluid is convected underneath, that is, into the separation wake. The separation wake extends from station LP:A through LP:2, as is shown in the separation cross-section, figure 2b.

Initiation of large-scale unsteadiness. At $t \approx 4.5s$, the shear-layer instability catches up with the viscous response. The shear layer rolls up and sheds in a dramatic and vigorous fashion (figures 4a and 4b). Accordingly, $\langle u'u' \rangle$-profile histories exhibit a pronounced alteration at this time.

Arrival at quasi-steady state. The $\langle U \rangle$-velocity profile histories, figures 4a and 4b, reveal an almost unchanging profile from $t \approx 7.5s$ until the end of the cycle, when suction is released. Although these profiles appears steady, they conceal perpetual unsteadiness in the steady-state structure of three-dimensional separation. Details of the physics and structure of the separation are better understood by considering profile histories of double product terms.

After $t \approx 7.5s$, the broad $\langle u'u' \rangle$-profile at LP:1 (figure 5a) has collapsed to a narrow peak. The narrow peak could be indicative of regular vortex roll-up or of flapping of the shear layer in the y-direction. The $\langle v'v' \rangle$- and $\langle u'v' \rangle$-profile plots (figures 6a and 7a, respectively) convince us of the latter explanation. For example, were vortex roll-up the dominant mechanism, then the $\langle v'v' \rangle$-profiles at LP:1 should show a peak similar to $\langle u'u' \rangle$ during the quasi-steady state. A low-frequency flapping of the shear layer at this location would result in the observed peak in $\langle u'u' \rangle$-profiles and flat $\langle v'v' \rangle$- and $\langle u'v' \rangle$-profiles.

In contrast, downstream at the location at LP:2, the broad peak in the $\langle u'u' \rangle$-profile persists throughout the quasi-steady state (figure 5b). This broad peak also appears in $\langle v'v' \rangle$- and $\langle u'v' \rangle$-profiles (figures 6b and 7b). The consistent peak throughout the double product profiles confirms that at this streamwise location, vigorous activity in the x- and y-directions trades high-velocity fluid in the outer flow with low-velocity fluid that was near the wall. In other words, spanwise vortices are passing through this streamwise

location. Evidently, the location of vortex roll-up has traveled downstream of LP:1 to a final position upstream of LP:2.

Thus the quasi-steady state includes a regular roll-up and shedding of vorticity from the separated shear layer that occurs between LP:1 and LP:2. Flow visualization confirmed that well-defined vortices began to roll up near LP:1 and shed through LP:2.

Conclusions

This experimental study on the fluid dynamics of unsteady, three-dimensional flow separation has broadened the understanding of the time behavior of these flows.

A definition for unsteady and three-dimensional separation has been adopted that is consistent for all such flows. This definition follows the suggestions of Legendre, Tobak and Peake. Although a controversy has arisen because of the differing definitions, it is found that all phenomena are adequately addressed by all.

The dominant processes of the development of a three-dimensional separation can be divided into four stages for various zones of the flow structure. Some of these zones experience all of the stages as the separation develops under an impulsively imposed adverse pressure gradient.

The four stages in the development of three-dimensional separation are the initial inviscid response, the breakaway of the shear layer, initiation of large-scale unsteadiness, and the quasi-steady state.

Acknowledgements

The authors gratefully acknowledge support by the Office of Naval Research under contract N00014-84-K-0232, which was monitored by Dr. S. Lekoudis.

Bibliography

DIDDEN, N. & HO, C.M. 1985 'Unsteady separation in a boundary layer produced by an impinging jet.' *Journal of Fluid Mechanics,* **160**, pp. 235-256.

KOROMILAS, C.A. & TELIONIS, D.P. 1980 'Unsteady laminar separation: an experimental study,' *J. Fluid Mech.* **97**, part 2, pp. 347-384.

LEGENDRE, R. 1982 'Regular or Catastrophic Evolution of Steady Flows Depending on Parameters.' *Recherche Aérospatial* 1982-4:41-49.

PAULEY, L.L., MOIN, P. & REYNOLDS, W.C. 1988 'A Numerical Study of Unsteady Laminar Boundary-Layer Separation.' Stanford University Dept. of Mech. Engineering: Thermosciences Division. Report No. TF-34.

PERRY, A.E. & HORNUNG, H. 1984 'Some Aspects of Three-dimensional Separation, Part II: Vortex Skeletons.' *Zeitschrift für Flugwissenschaften und Weltraumforschung.* **8**, Heft 2:155-160.

TOBAK, M. & PEAKE, D.J. 1982 'Topology of Three-Dimensional Separated Flows.' *Annual Review of Fluid Mechanics.* **14**: 61-85.

Tunnel Geometry		
Dimension	Value	Comments
L, x-Length (total)	3.66 m	
x to LP:B, chord	0.575 m	
x to LP:D	0.613 m	Suction port begins
x to LP:1	0.651 m	Suction port ends
x to LP:2	0.689 m	
H, y-Depth (total)	0.129 m	
W, z-Span (total)	0.356 m	
width of suction port	38.1 mm	Port centered in span

Flow Conditions		
Quantity	Value	Comments
U_0	0.217 m/s	Inlet flow velocity
Q, (total)	0.0100 m^3/s	Volume flowrate
for Zero Pressure Gradient		
θ at LP:B	0.00125 m	Momentum thickness
θ at LP:1	0.00139 m	
θ at LP:2	0.00143 m	
for Suction		~16%
Q	0.00156 m^3/s	Volume flowrate
dU	0.0334 m/s	Least-squares fit
max. dC_p/dx	2.52 $1/m$	Gradients of Press. Coeff.
max. dC_p/dz	0.266 $1/m$	from potential flow est.

Table 1. Tunnel geometry and flow conditions.

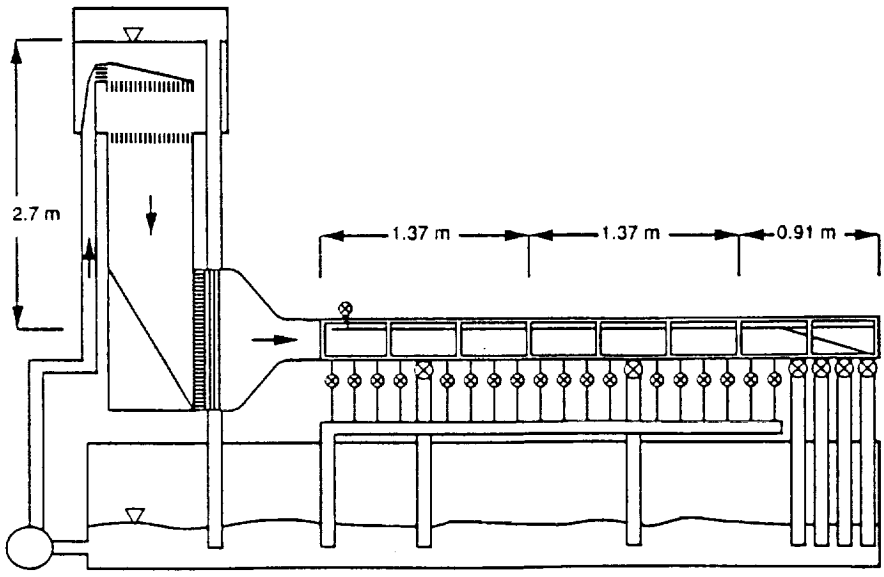

Figure 1: The Stanford unsteady boundary-layer research water tunnel.

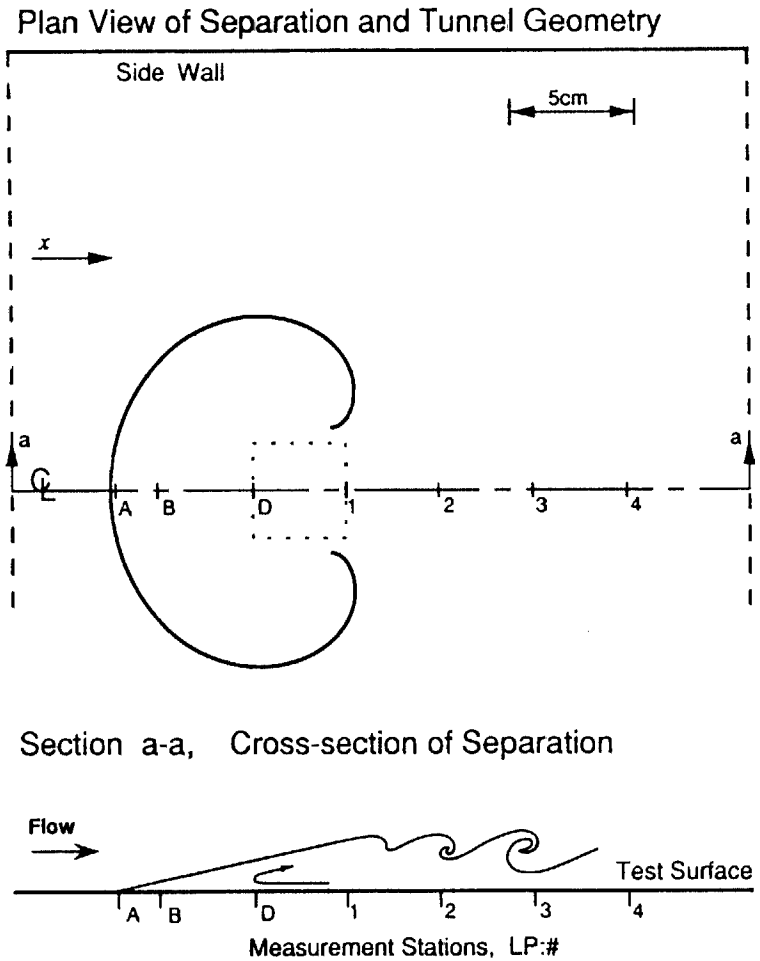

Figure 2: A schematic of tunnel geometry and separation structure shows location of measurement stations. The separation wake, composed of sluggish fluid, resides within the Owl-face structure between stations A and 1.

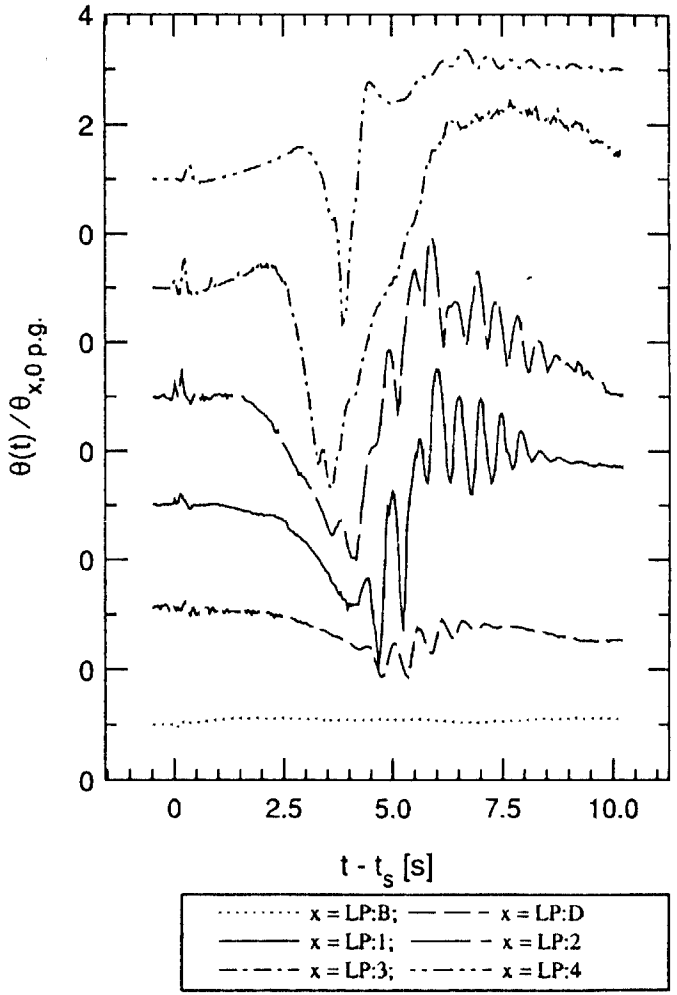

Figure 3: Histories of the momentum thickness, θ, along the centerline of the developing separation. The instantaneous momentum thickness becomes negative at several locations. Values are normalized to the value of the local momentum thickness during zero pressure-gradient conditions.

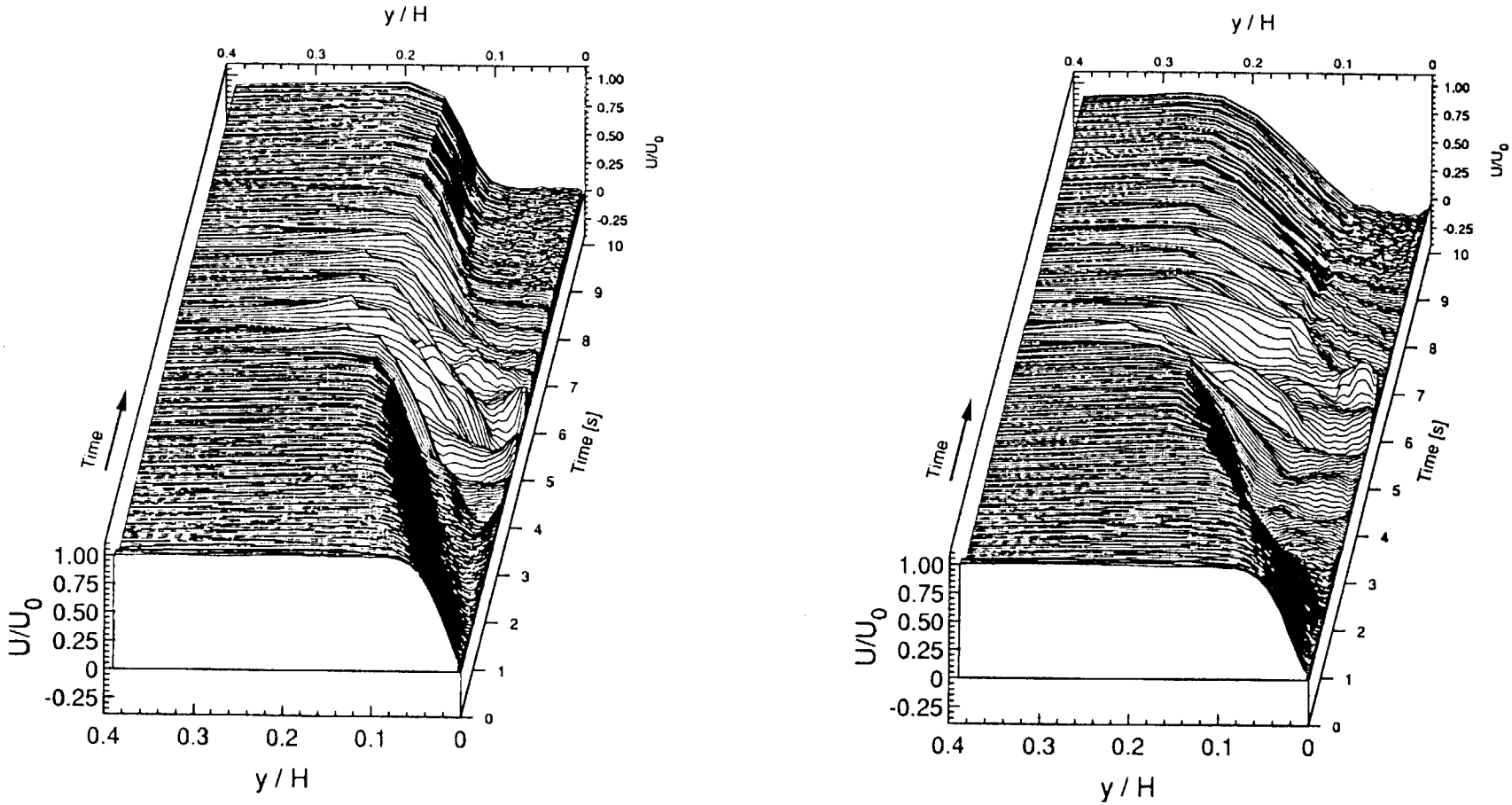

Figure 4: Evolution of the phase-averaged $\langle U \rangle$-velocity profiles from the instant the adverse pressure gradient is applied: (a) is at LP:1, (b) is at LP:2.

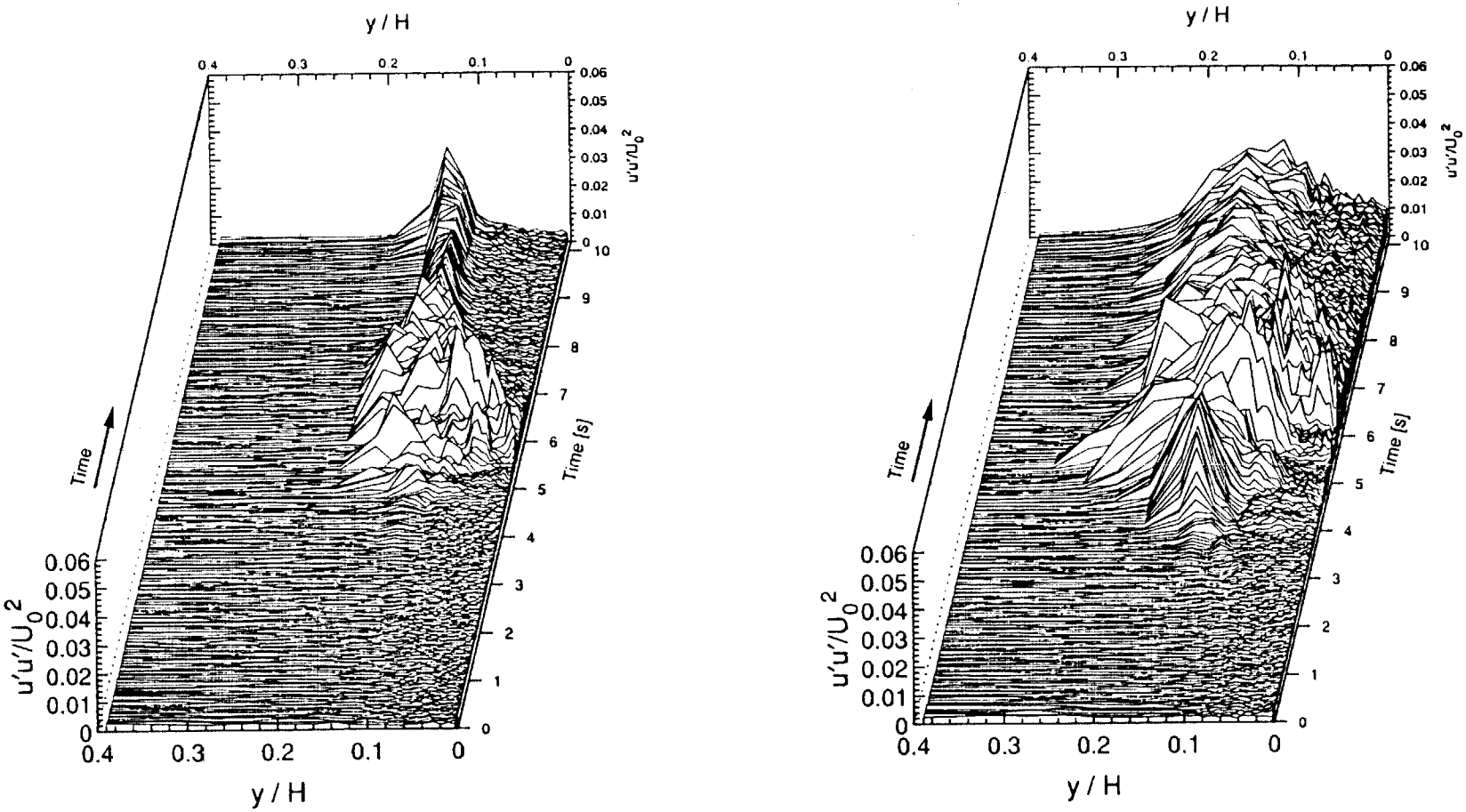

Figure 5: Evolution of the phase-averaged $\langle u'u' \rangle$-velocity profiles from the instant the adverse pressure gradient is applied: (a) is at LP:1, (b) is at LP:2.

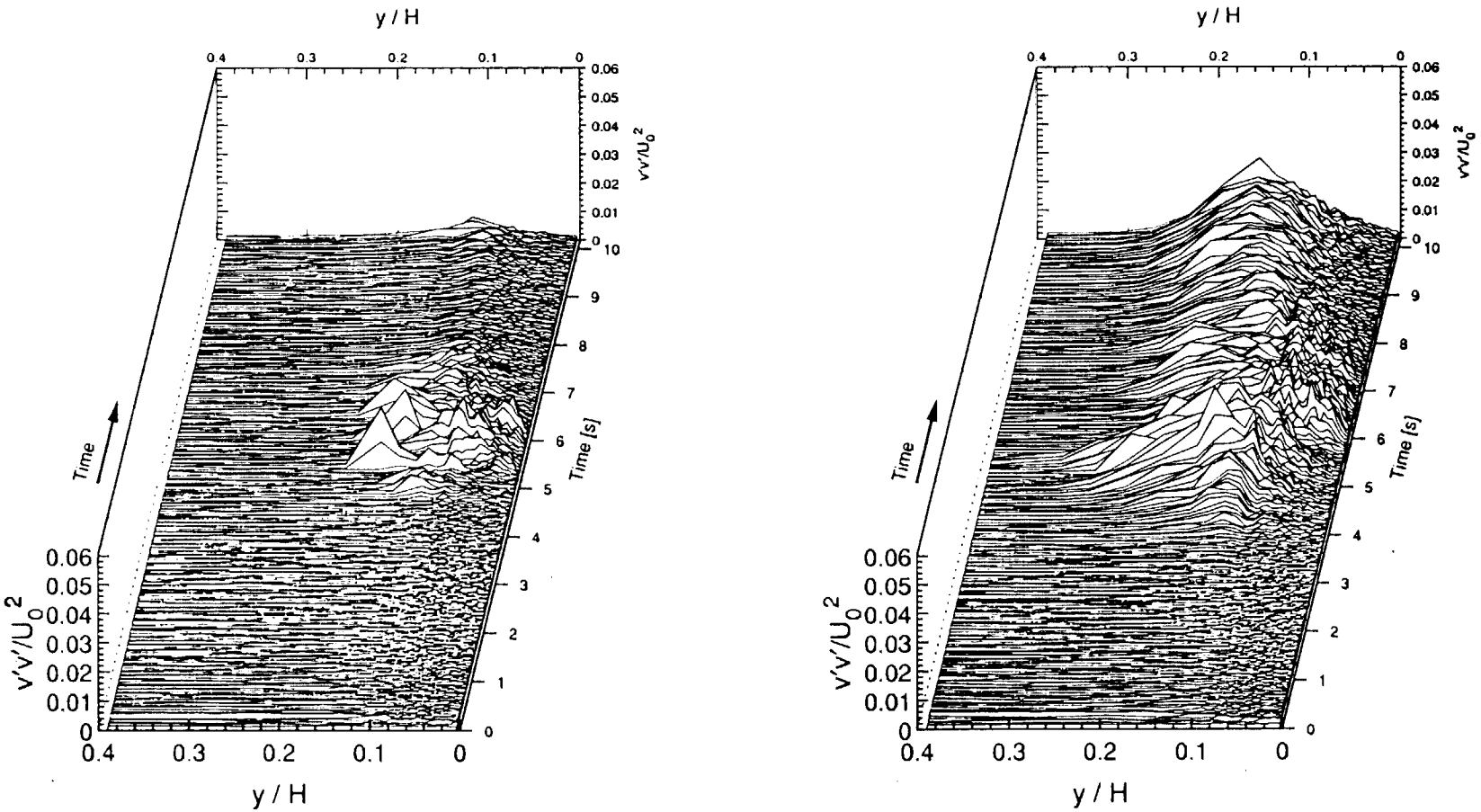

Figure 6: Evolution of the phase-averaged $\langle v'v' \rangle$-velocity profiles from the instant the adverse pressure gradient is applied: (a) is at LP:1, (b) is at LP:2.

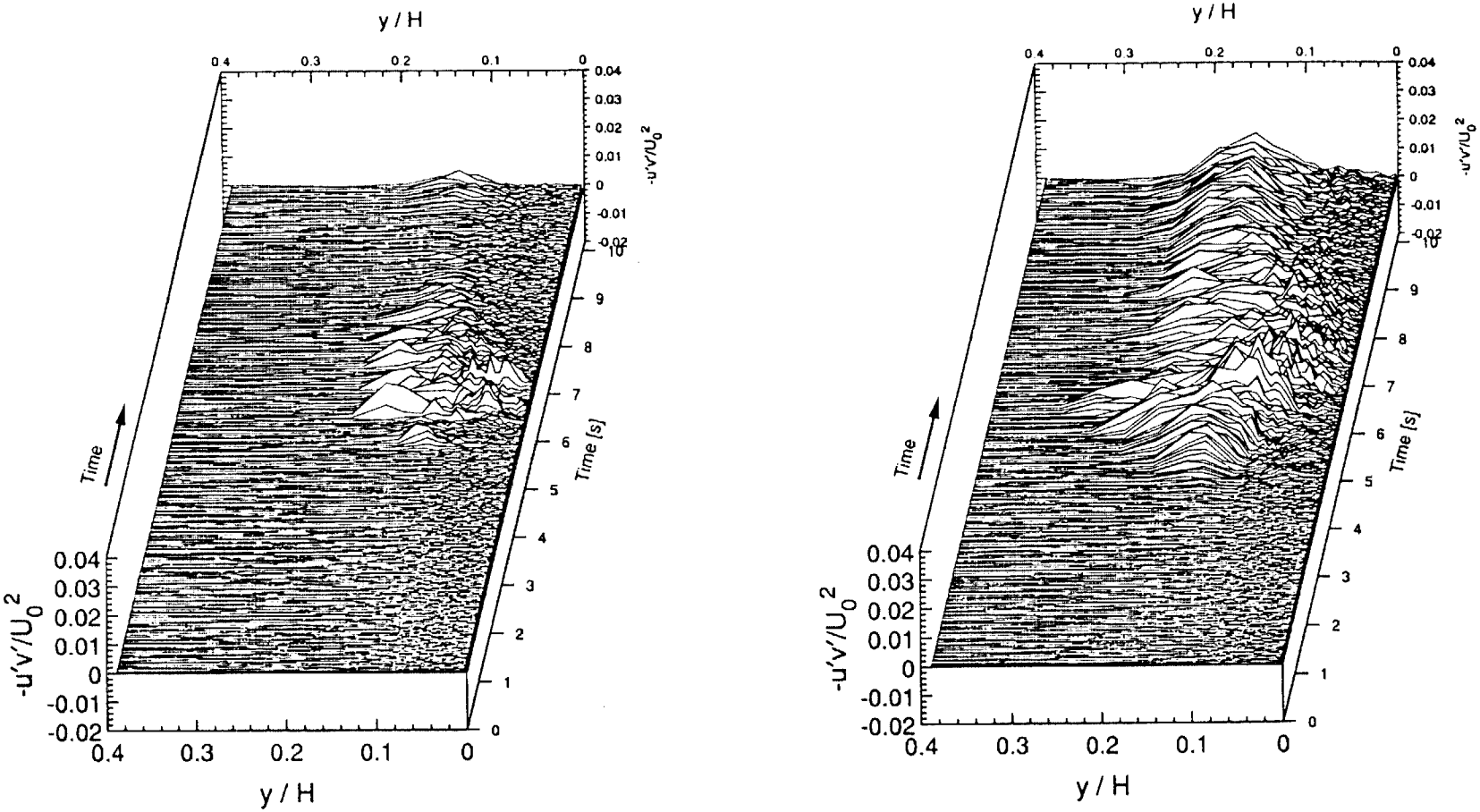

Figure 7: Evolution of the phase-averaged $\langle u'v' \rangle$-velocity profiles from the instant the adverse pressure gradient is applied: (a) is at LP:1, (b) is at LP:2.